Applied Energy 374 (2024) 124055

Contents lists available at ScienceDirect

Applied Energy

journal homepage: www.elsevier.com/locate/apenergy

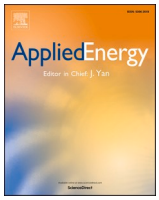

A hierarchical test benchmark of integrated energy system in Northeast China

Xue Li [a], Junyan Shao [a], Tao Jiang [a,*], Houhe Chen [a], Yue Zhou [b], Rufeng Zhang [a], Hongjie Jia [c], Jianzhong Wu [b]

[a] Department of Electrical Engineering, Northeast Electric Power University, Jilin 132012, China
[b] School of Engineering, Cardiff University, Cardiff CF24 3AA, UK
[c] Key Laboratory of Smart Grid of Ministry of Education, Tianjin University, Tianjin 300072, China

HIGHLIGHTS

- Scalable benchmark configurations of LIES and CIES are developed and shared.
- Utilization of energy flow calculation is extended to the hierarchical test benchmark.
- Derivative studies such as OEF, CEF, PEF, and DEF are computed.

ARTICLE INFO

Keywords:
Urban energy system
Test benchmark
Distribution network
Micro energy system
Hydrogen system
Heating distribution network

ABSTRACT

To move from one-off restricted utilization of custom technologies upgrade to joint implementations at scale, demanding a recognized standard test benchmark for plausibility inspection. Therefore, the test benchmark of integrated energy systems (IESs) needs to exhibit generality and universality to adapt to and match the state-of-the-art research. The publicly available test benchmark developed in this paper consists of two levels: i) Local integrated energy system (LIES), which encompasses an electricity distribution grid and a primary heating network; ii) Community integrated energy system (CIES), which incorporates a microgrid and a secondary heating network in a campus. The database of the test benchmark stems from investigations and mirrors the physical assets of a real-urban energy system and takes into account the virtual deployment of future planning for wind power and hydrogen systems. LIES showcases key features of the IES located in a densely populated area, and CIES is a critical load encapsulated in LIES. The parameters and details of the database shared in the appendix involve cable impedance, pipeline parameters, electrical and thermal loads, etc., supporting independent access and the customized reconfiguration for the simulation and computation of emerging technologies. The practicality and validity are examined through the multiple instantiated basic energy flow calculations and myriad derivative calculations.

1. Introduction

As a promising revolutionary program, integrated energy system (IES) is expected to gain more popularity in the next few years, even decades, and widely address the challenges associated with the distribution and conversion of energy [1]. IESs unprecedentedly emerge as a hot research direction, owing to the myriad functions and diverse energy provisions [2]. Subsequent to progressive evolution, IES is defined as a wise and prudent deployment observed from both local and global viewpoints, optimally generating electricity, heat and gas to meet the diverse demands of users [3,4]. IESs exhibit strong performance in energy coordination and redistribution, addressing the various challenges that are hard to solve through conventional independent energy sectors [5].

Despite the surge in interest, the implementation and promotion of IESs are not only associated with the integration of state-of-the-art technologies but also standardized tests [6]. However, numerous existing test cases are hard to promote, owing to the intrinsic shortcomings, such as various energy discrepancies and small-scale energy implementation in communities. These test systems are misaligned with real-world scenarios. Indeed, developing a generalized test benchmark

* Corresponding author.
E-mail address: tjiang@neepu.edu.cn (T. Jiang).

https://doi.org/10.1016/j.apenergy.2024.124055
Received 25 March 2024; Received in revised form 16 June 2024; Accepted 25 July 2024
Available online 2 August 2024

Nomenclature

Indices and index sets

i/j	Set of branch start/end nodes in a distribution network
n_e	Set of the total bus number of the power system
n_h	Set of the total node number of the thermal system

Variables

U_i/U_j	Voltage of the bus i and j
P_i/Q_i	Active and reactive power at bus i
δ_{ij}	Voltage phase angle of bus i-j
G_{ij}/B_{ij}	Conductance and susceptance of branch i-j
$\dot{\boldsymbol{m}}$	Matrix of pipeline water flow
$\boldsymbol{m_q}$	Nodal injection water flow column
$\boldsymbol{h_f}$	Pressure head loss
$\boldsymbol{T_s}$ / $\boldsymbol{T_o}$	Temperature matrix of injections and outflows of water
T_{start} / T_{end}	Water temperature at the start and end of the pipe
$\dot{\boldsymbol{m}}_{\text{out}}$ / $\dot{\boldsymbol{m}}_{\text{in}}$	Matrix of outflows and injections at the nodes
$\boldsymbol{T}_{\text{out}}$/ $\boldsymbol{T}_{\text{in}}$	Matrix of Nodal outflow and injected water temperature
ϕ_{CHP}	Total power output of CHP
$P_{\text{CHP,e}}$	Power output of CHP
$\varphi_{\text{CHP,h}}$	Thermal output of CHP
$P_{\text{EB}}/\Phi_{\text{EB}}$	Input electrical power and output thermal power of EB

Parameters

$\boldsymbol{A_h}$	Node pipeline association matrix
$\boldsymbol{B}$	Loop branch correlation matrix
$\boldsymbol{K}$	Resistance coefficient matrix of the pipeline
C_{p}	Specific heat capacity of water
$\boldsymbol{\varphi}$	Load matrix of the nodes
T_{a}	Environment temperature
λ	Pipeline constants
L	Length of the pipeline
γ_{eh}	Thermal/electric output rate
$\phi_{\text{CHP,min}}$ / $\phi_{\text{CHP,max}}$	Maximum and minimum of output power of CHP
α	Thermal efficiency of EB
H_{g}	High calorific of EB
$\Phi_{\text{EB,max}}$	Maximum output power of EB

Abbreviation

IES	Integrated energy system
LIES	Local integrated energy system
CIES	Community integrated energy system
CHP	Combined heat and power plant
P2H	Power to hydrogen
EB	Electric boiler
PV	Photovoltaic
ESS	Energy storage system
EF	Energy flow calculation
OEF	Optimal energy flow calculation
CEF	Continuous energy flow calculation
PEF	Probabilistic energy flow calculation
SNB	Saddle node bifurcation

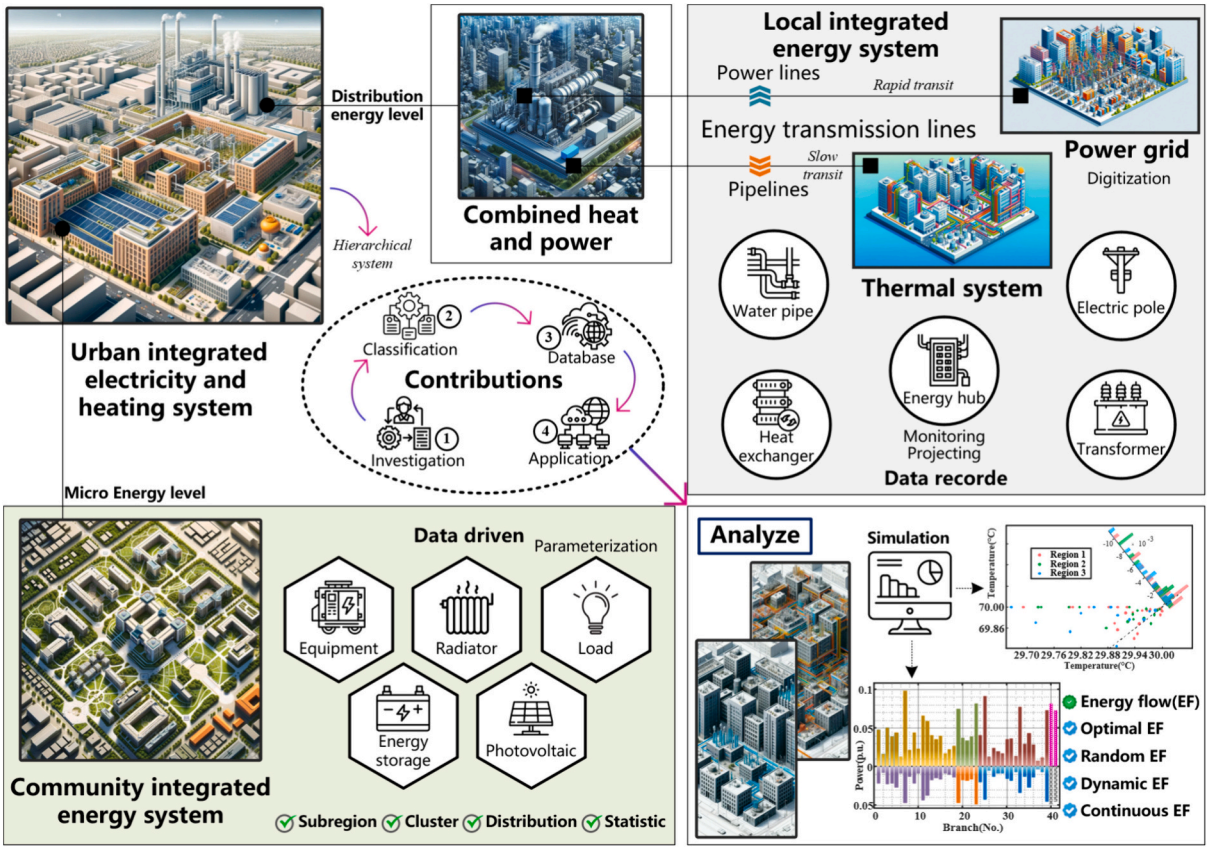

Fig. 1. Main contributions of the paper.

Table I
Comparison of different cases for integrated energy system.

Literature	Heating system	Power system	Size (bus/node)	Capacity
[17] [18]		√	33	12.02 (p.u.)
[19]		√	118	4374.82 (p.u.)
[20]		√	57,118	1278.66 (p.u.)
[21,22]	√	√	300/324	23,935.38 (p.u.)
[23]	√		13,151,33	3200 (p.u.)
[24,25]	√	√	22/23	1060 (p.u.)

demands an extensive amount of prior knowledge and necessary action, including the parameterization and digitization of numerous devices in IES.

Parameterization is a simplified process that involves showcasing the various properties of IES, such as capacity and efficiency, in parameter form [3]. These parameters may be either quantitative—like the power plant's generating capacity or a transmission line's loss percentage—or qualitative, such as the theoretical conversion efficiency. This process highlights the simplifying of complex systems and facilitates the comparison of technological implementations or test-type simulations with multiple conditions.

Digitization involves the implementation of digital technologies for recording, storing, and analyzing the data and operational processes of IES [1]. This action encompasses the deployment of sensors for real-time data collection and the application of software tools for system modeling and simulation, and the leveraging of information and communication technologies for the remote monitoring and management of energy systems.

Thus, this study contributes a real-urban energy test benchmark for mirroring the real-world energy system via parameterization and digitization of physical assets. This paper presents multi-dimensional data encapsulating the characteristics of the energy device in the appendix, creating a configurable and scalable test base for the myriad demands and various requirements of multiple IES research. The benchmark also incorporates uncertain renewable energy resources, expanding the range of applications to match the emerging problems of IES. The outlines and main contributions in this paper are illustrated in Fig. 1.

The main contribution of this paper is illustrated in Fig. 1. Substantial effort has been invested in the pre-processing of data in this work, including data collection, speculation, validation, and correction. This paper rededicated a standardized test benchmark for researchers. The proposed test benchmark comprises a local integrated energy system (LIES) and a community integrated energy system (CIES). The fundamental properties of the test benchmark are hierarchical, and each level of the system is available to access independently. Similarly, independent electrical or heating systems from each level also serve as a benchmark for decoupled computing and advanced study.

Combine heat and power plant (CHP) and electric boiler (EB) are deployed in the test system. As the core of a third-generation energy system [7], CHP is the critical connection of the subsystems to generate multi-energy in LIES. EB offers a unidirectional energy source within CIES, enabling the isolated, non-centralized heating buildings may be available to be heated in winter. Furthermore, the small-scale installation of photovoltaic (PV) and energy storage systems (ESS) also creates a flexible solution to the energy provision in the CIES, due to the degradation and retirement of conventional energy plants. With all these benefits, the functional and scalable energy system may serve as the representative candidate benchmark to evaluate frontier research. Hence, the primary mission of this task is to share the data of LIES and CIES and evaluate the performance of frontier technologies.

In alignment with the intent of prior work, it is imperative to summarize the investigation and inspection of the electric benchmarks proposed by IEEE. IEEE has consistently shared a series of test benchmarks [8]. These publicly accessible datasets serve as valuable resources for the engineering community summarized in Table I, empowering a more profound comprehension and understanding of how emerging technologies and operational solutions influence the cost and performance of the electric power system. Accumulation over time, the IEEE test benchmarks have developed into recognized references and simulation basics for analyzing electric system operational strategies and issues beyond just mirroring or representing physical assets of the real-world power system [9,10]. These test benchmarks are shared to illustrate configurations encountered in various scenarios. Therefore, this research aims to uphold the tradition of IEEE, classifying a wide range of physical assets sorting out the different types of physical systems, and creating a digitized database for the components of an integrated energy system. This paper develops a hierarchical benchmark that strives to mitigate the disadvantages of existing nonstandard cases, addressing the challenge of unreasonable connections and the mismatch of energy levels between energy subsystems.

Despite the surge of interest, devising a universally perfect test benchmark is infeasible. Akin to the task by IEEE, the test benchmark serves as a foundational reference, customizing a baseline and reference for evaluating the operations and performance of various technologies in IES. The main characteristics of the benchmark are as follows:

(1) A hierarchical IES benchmark including a local integrated energy system (LIES) and a campus integrated energy system (CIES) is developed. A hydrogen system and wind power system are pending in connection to bus 12 on the LIES.
(2) The database within the benchmark is shared and accessible, offering critical simulation parameters encompassing diverse loads, installation capacities, pipe parameters, and transformation parameters. Each level within the benchmark can be individually accessed and customized casually, benefiting flexibility and availabilities in frontier research investigations. The database fully covers most computing requirements.
(3) The multiple results of the energy flow calculations (EF) and dynamic energy flow calculations (DEF) for the benchmark are calculated, and the optimal energy flow calculations (OEF), continuous energy flow calculations (CEF), and probabilistic energy flow calculations (PEF) of the benchmark are further explored. These calculations are to corroborate the availability of the dataset [11].

The remainder of this paper is organized as follows. In Section 2, a brief history of the existing IES and some of the features in the original system are discussed. Section 3 presents the details of the test system. Section 4 tests the system under different conditions via essential functions. Finally, Section 5 concludes the paper.

2. History of the existing integrated test system

The exploration of IES can be traced back at least a decade or more [12]. The inception of this research domain commenced as a derivative research of gas turbines. After explosive development, IES has garnered a focal point in many applications, owing to a boost in interest in investigations of gas turbines and electric heat boilers. This approach involves electric and heating systems as interrelated dynamical systems, evolving through their respective energy carriers. Subsequently, various units in an extensive portfolio of power and heat systems are abstracted into nodes, buses, branches, pipes, etc. This can be simplified and used to perform various types of calculations at the network level.

The contribution of previous work depends in part on investigations. A portion of the data is derived directly from the server of CHP, the operator records and gathers observational data derived from various assets via myriad sensors or pattern identifiers. Indeed, the database is utilized to update and accurately mirror the evolving physical system consistently. This data functions as multi-dimensional synergistic coupling, involving physical design, data collection, computational

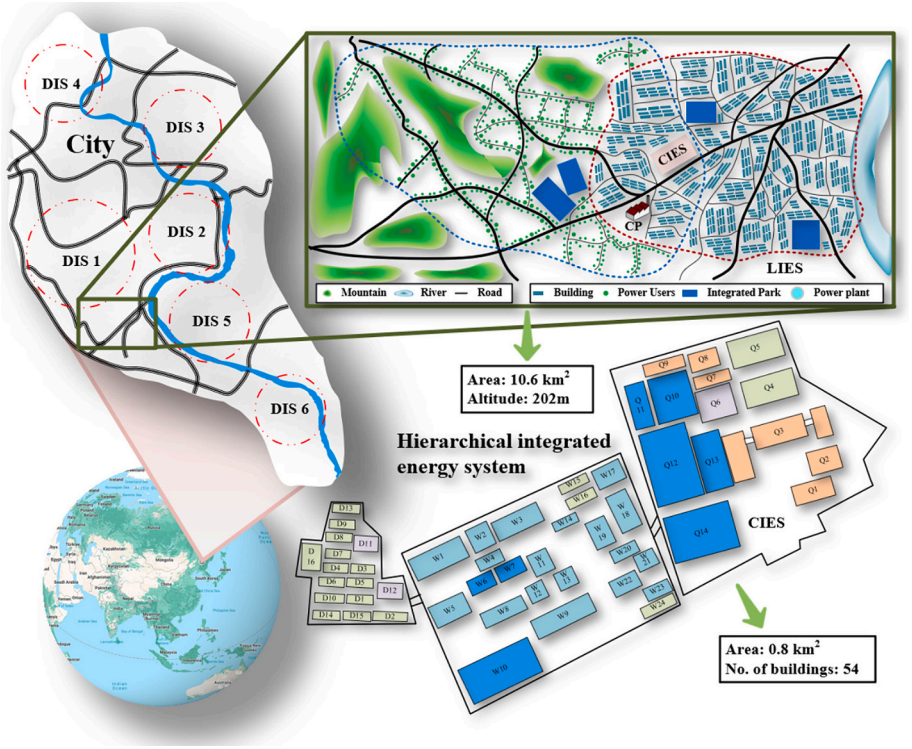

Fig. 2. Location and geographic map of the test benchmark.

models, and decision-making processes. Subsequently, the IES operator unlocks the potential to leverage the up-to-date database for multiple purposes, such as analysis, prediction, optimization, and control.

In previous research, several authors tried randomly creating a one-off non-formal connection utilizing a standard electrical system and another possible heating system. Since it is not a real-world system, these systems exhibit a variety of sizes and energy levels [13–16]. This paper begins with a review of previous studies.

2.1. Electric system

The power systems in previous case studies are generally derived from IEEE standard cases. This showcases widely acceptable and high performance. The case proposed by IEEE exhibits both flexible and scalable. The IEEE 33-bus standard benchmark is widely prevalent in both IES studies and other research, such as the electricity market and energy optimal scheduling [17–19]. Evolving over time, lower energy level, poor expandability, and other insurmountable challenges have gradually been exposed.

Many researchers have transitioned the case study to the advanced test benchmark, which is rigorous yet flexible, such as IEEE 118 [20] and IEEE 300 [21]. Some investigators also sought to explore a real-world case of combined power and heating systems [22]. Popular power test benchmarks are frequently utilized for energy flow calculations and other studies. However, sustained utilization of these benchmarks may be terminated triggered by the energy mismatch.

2.2. Heating system

Motivated by a similar inspiration, a few heat network test cases are developed incrementally. [23] studied extensive exploration of the technical, economic and environmental potential of heating facilities within the Stockholm district heating network versus seasonal heat storage facilities. In addition, [24] undertook a validation simulation based on a conventional district heating system in Germany. Furthermore, [25] engaged in a dynamic simulation and energy-economic analysis of a novel solar district heating, cooling, and domestic hot water system situated in southern Italy. Meanwhile, [26] summarized data from district heating systems in Finland and investigated the optimal design and comparison of centralized and semi-decentralized community-scale solar district heating systems. Similar heating networks are employed to compute the hydraulic and heating energy flow in much research.

The aforementioned cases have been applied and examined within a limited scope of applications. Small-scale systems appeared only in specialized journals rather than being recognized and referenced.

To the best of the authors' knowledge, the above cases are not promising for implementation and utilization at scale due to the single topology and impractical connection. The following features are the main aspects incorporated in the test benchmarks presented in this paper:

(1) Radial and loop distribution systems with multiple levels.
(2) Distribution networks and microgrids.
(3) Primary heating system and secondary heating system.
(4) Deployment of renewable energy generation and heating coupling unit within the system.

As aforementioned, one-off customized systems are obviously hard to promote for various applications [27]. To fill the research gap, this paper then delves into the exploration and demonstration of a more functional and valuable real-world system characterized by applicability, scalability, and energy interoperability [28]. To this end, the proposed test benchmark should empower researchers to access each level of the systems to respond to their unique requirements. Furthermore, the benchmark should be sufficiently complex to approach the scale of challenges likely to be encountered in modern integrated energy systems, as shown in Fig. 2.

3. Test benchmark of LIES and CIES

The outcome of this paper is to showcase a practical and scalable test

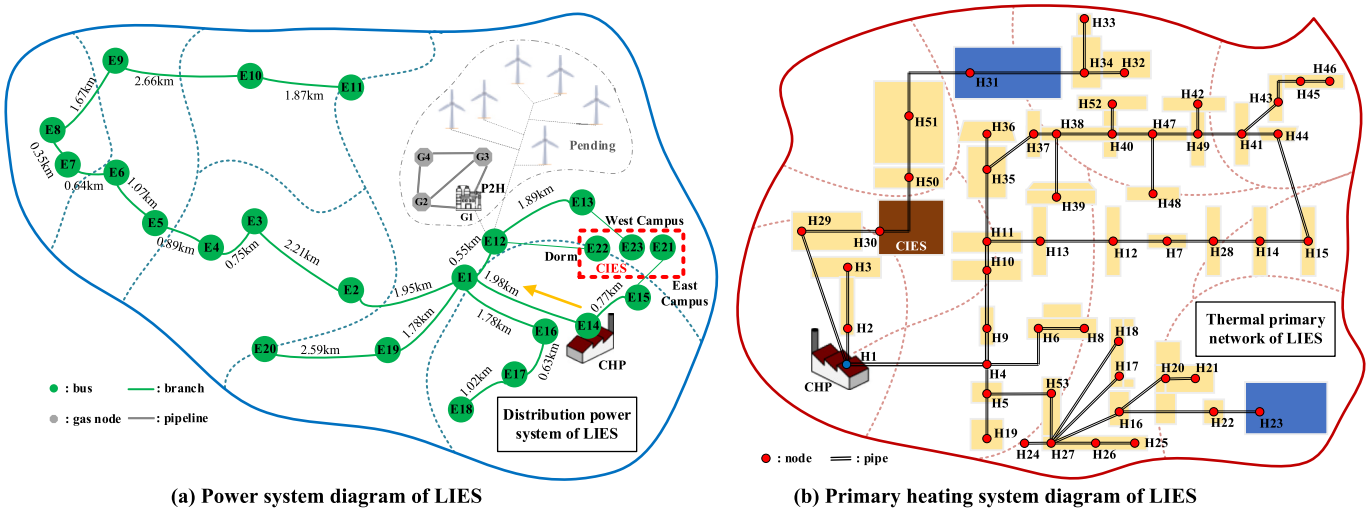

Fig. 3. Geographic diagram of the power system and heating system of LIES.

Fig. 4. Micro-gird and heating system diagrams of CIES.

benchmark. This paper highlights the data details of the test benchmark in Fig. 2. The data of the test benchmark nearly encompasses all the attributes of existing power systems and heating systems. Even in applications of checks and tests for complex computational models, the proposed benchmark proves to be effective and robust for extensive and future research.

3.1. *Candidate for test benchmark*

Fig. 3 depicts the geographical map of the proposed test benchmark. The candidate area is a suburban city in northeastern China in the geometric center of northeast Asia. The region's climate features continental monsoon characteristics, marked by four distinct seasons, including snowy and rainy periods. The area features diverse

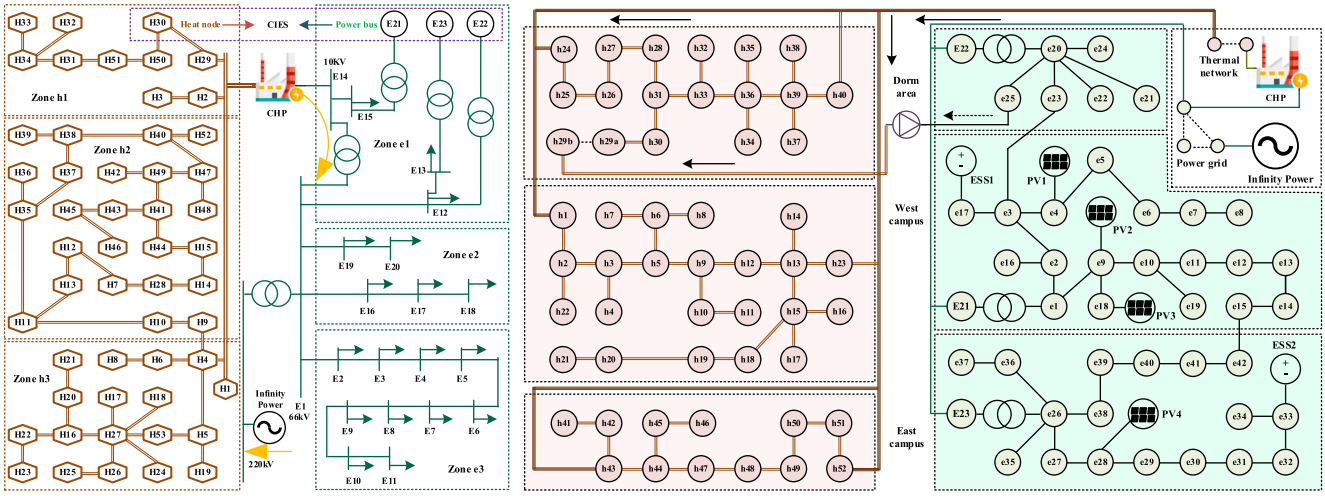

Fig. 5. Topological diagram of LIES and CIES.

topographical elements, such as mountains, rivers, plains, and more.

The test benchmark of LIES covers a geographic spanning area. LIES encompasses residential buildings, schools, and self-heating customers. The area is loacated on the border between urban and rural areas in the candidate city. Residential buildings and shopping centers rely on heating systems and electricity supply, while rural users leverage biomass burning to maintain heating in winter. Furthermore, a CHP within the region offers both heat and electricity. The development of test benchmarks involves data calibration for primary purposes and experimental data tests to enhance the performance of the system.

In Fig. 3 (a), set E = {E1, E2, E3, … E23} indicates the buses of the distribution power system. In Fig. 3 (b), set H = {H1, H2, H3, … H52} indicates the nodes of the primary heating system. LIES also incorporates local observations and a centralized database derived from various sensors and the long-term operational server within the CHP. In addition, Fig. 3 (a) showcases a future plan for hydrogen systems and wind power. The campus operator of CIES utilizes an energy management system to record facility parameters and details of the entire energy system, supporting the test benchmark calibrations. The CIES data exactly involve variable energy resources, such as distributed PV.

3.2. Geographic diagram of LIES

The schematic diagram of the LIES is shown in Fig. 3. In Fig. 3(a), the diagram displays the lengths of the branches and the connections between the load and the supply, along with the labels of the substations corresponding to specific local buildings in the area. Four electric lines are branched from the main transformer to feed this area. The CHP is linked to the main transformer with a voltage level of 66 kV. On the other end, it connects to bus 15, generating power to the east campus of CIES. The west campus and dorm are linked to the main transformer at Bus 13 and Bus 12. In the heating system shown in Fig. 3(b), the complexity level of the topology is noticeably higher than that of the power system, and return pipes share the same as the transmission pipes and are therefore omitted. The area covered by the diagram includes numerous buildings, a high school, and CIES. The area is primarily heated through three main pipes.

3.3. Schematic of CIES

CIES is likewise parsed and is shown in Fig. 4., dividing into two subsystems.

Here, the entire CIES is distinctly divided into three areas based on administrative criteria. In the power system depicted in Fig. 4, power is supplied to these three areas - east campus, west campus, and the dorm through three 10 kV transformers. PV and ESS are installed and deployed within the east and west campuses aids for the power supply.

Pipes are installed along the central area of the three campuses. The west campus notably features a loop structure, while both the dorm and the east campus are connected at two interfaces within the heating network. It's worth mentioning that Dorm 16 is located at a higher elevation, disconnected from the heating system. EB is utilized to generate energy during the winter to ensure the temperature of Dorm reaches the standard. Two systems are coupled together in the CIES through this device.

3.4. Topology of LIES and CIES

Topology is remarkably more precise and observable for researchers. Therefore, this section has further redrawn the curves of branches and pipes into a topology diagram, transforming them into more easily identifiable lines. This operation has been applied to both LIES and CIES in Fig. 5. Both LIES and CIES are divided into various zones based on installation order and specific location. The heating system of LIES is categorized into three areas based on geographic location, while the electrical system is divided into three areas. Each area can be accessed and analyzed separately.

The respective campus district affiliation determines the principle of partition for CIES. The entire system can be reconfigured through the operation to support advanced computational programs.

This section introduced the topological and geographical structure of the LIES and CIES. The parameters of LIES and CIES are shown in Appendix A and Appendix B. For the type of the sheets: 1 denotes the power/heat load, 2 denotes the bus/node of the supply source with fixed output, and 3 denotes the balancing bus/node. The next section introduces the instantiated computational procedure to test the availability of the database.

4. Application of the benchmark

As a foundation, the paper contributes detailed descriptions of energy flow calculations and potential derivative calculations, demonstrating how benchmarks in different conditions can support multifunctional computations.

4.1. Energy flow calculation

The calculation model of the power system employs the traditional

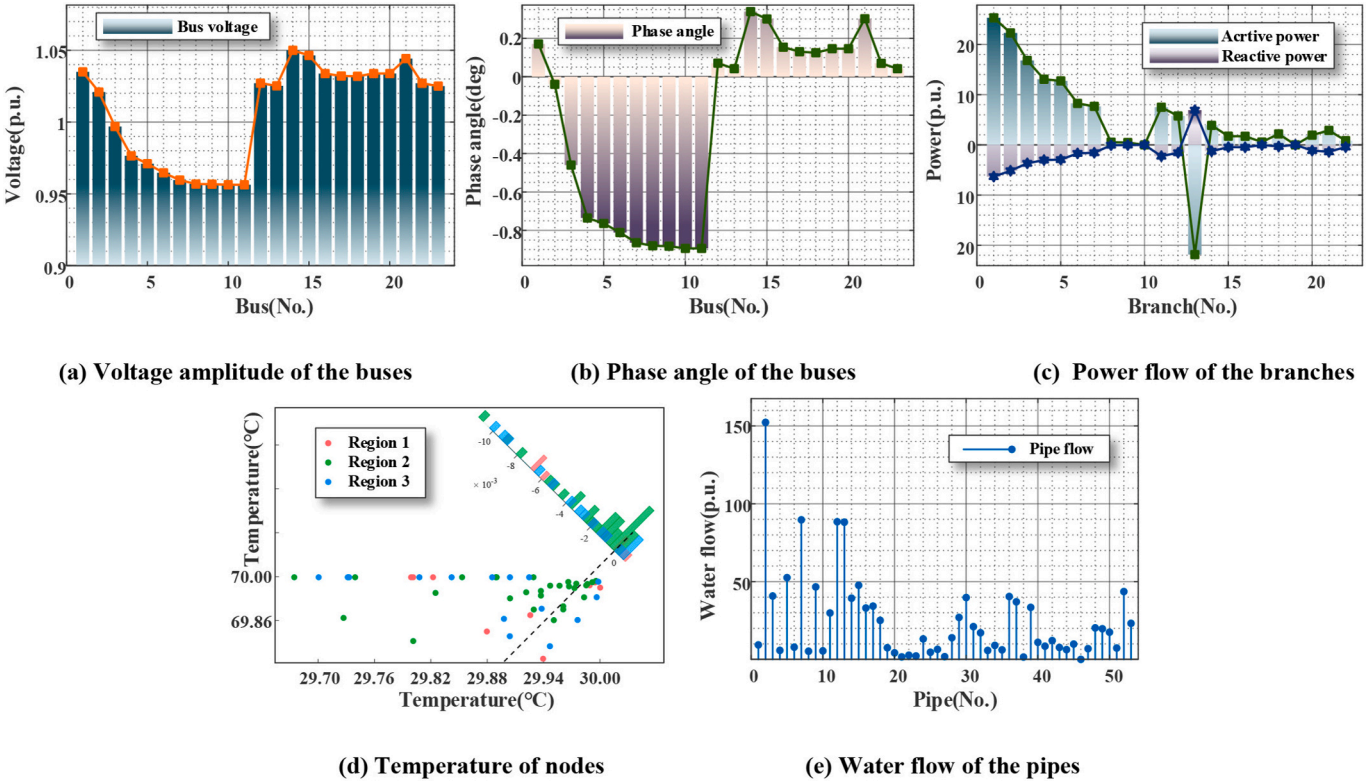

Fig. 6. Calculation of the energy flow in LIES.

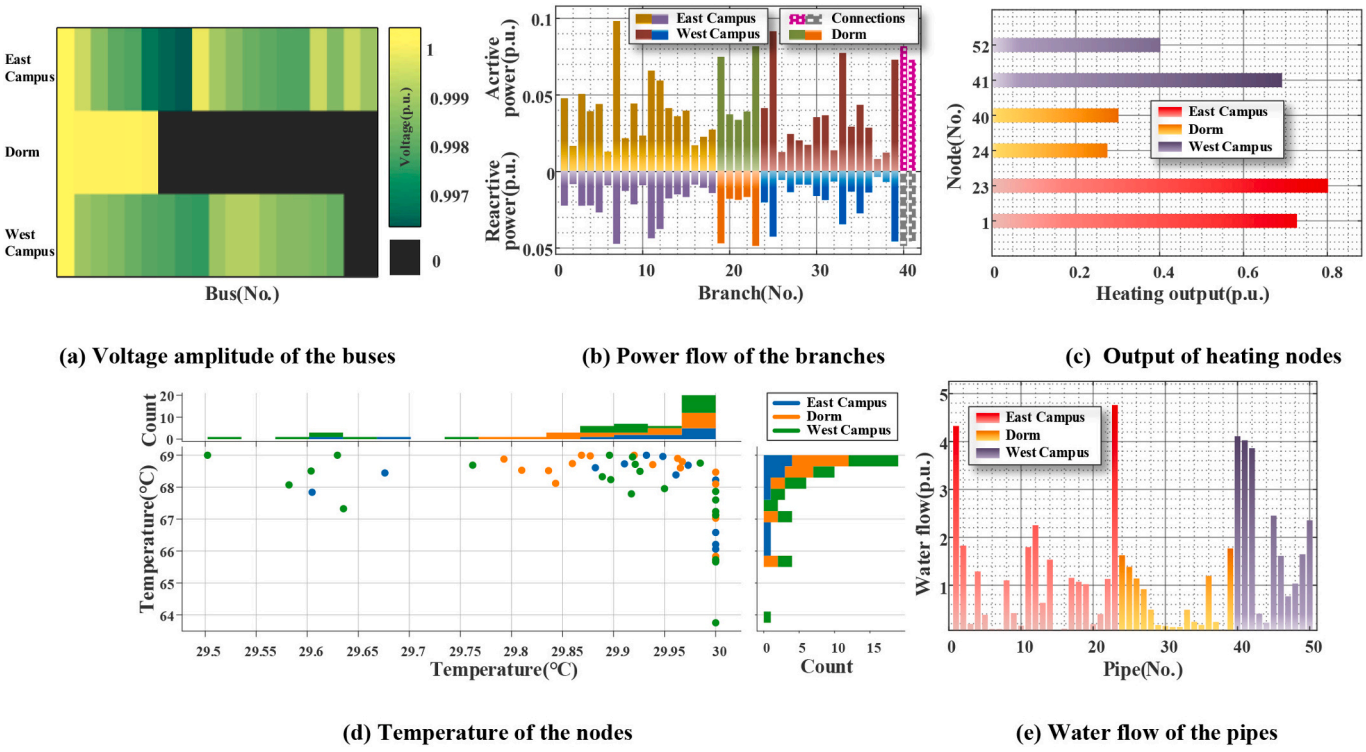

Fig. 7. Calculation of the energy flow in CIES.

AC model. In this aggregate formulation, each bus primarily encompasses four state variables: active power, reactive power, voltage magnitude, and voltage phase angle [29]. The formulation among these variables is as follows:

$$P_i = U_i \sum_{j=1}^{n_e} U_j \left(G_{ij} cos\delta_{ij} + B_{ij} sin\delta_{ij} \right) \tag{1}$$

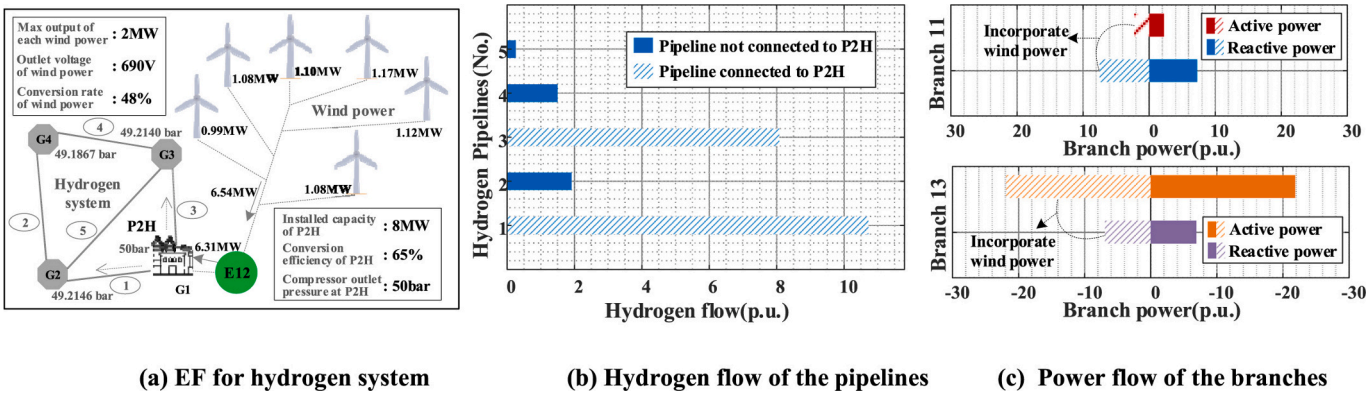

(a) EF for hydrogen system (b) Hydrogen flow of the pipelines (c) Power flow of the branches

Fig. 8. Calculation of the EF in CIES with wind power and hydrogen system.

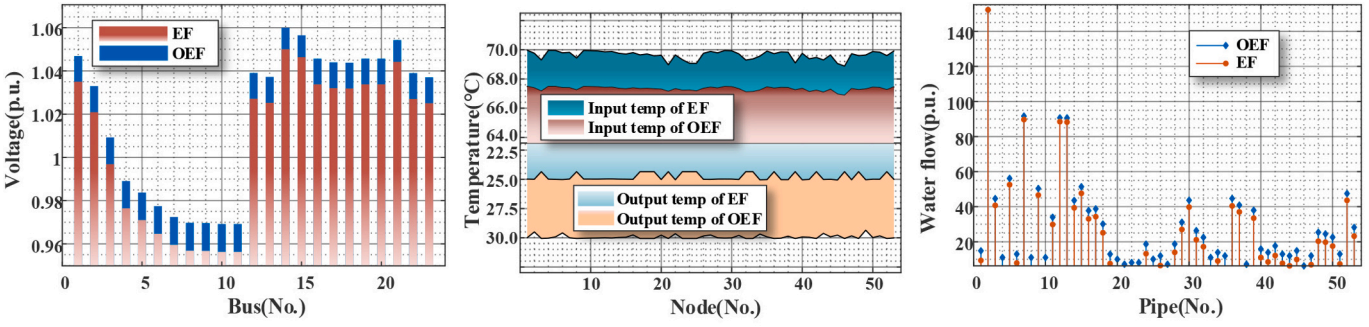

(a) Voltage amplitude of the buses (b) Node temperature (c) Water flow of the pipes

Fig. 9. Calculation of the optimization energy flow in LIES.

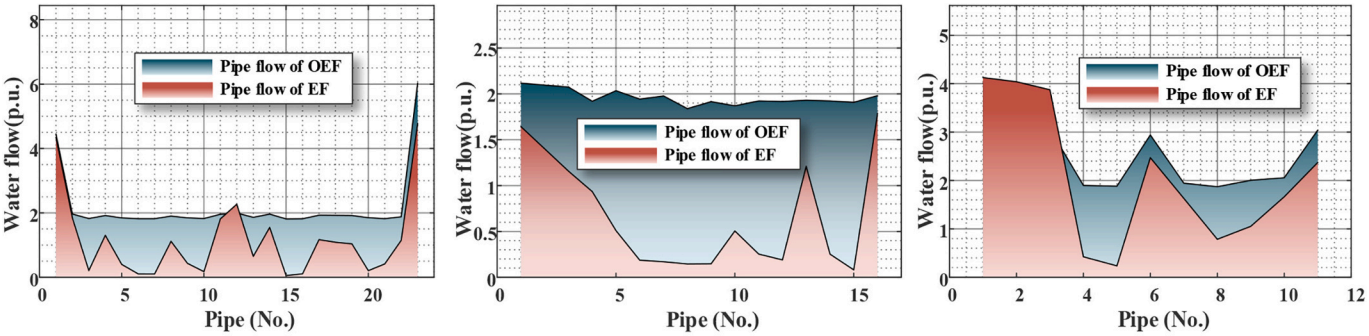

(a) Water flow of the west campus (b) Water flow of the dorm (c) Water flow of the east campus

Fig. 10. Calculation of the optimization energy flow in CIES.

$$Q_i = U_i \sum_{j=1}^{n_e} U_j \left(G_{ij} sin\delta_{ij} - B_{ij} cos\delta_{ij}\right) \tag{2}$$

The mathematical counterpart for the heating system utilizes a heating calculation model for urban pipeline networks, primarily consisting of hydraulic and heating models.

(1) The hydraulic model is concerned with the dynamics of the hot water in the pipe [30], which can be shown as:

$$\mathbf{A_h}\dot{\mathbf{m}} = \mathbf{m_q} \tag{3}$$

$$Bh_f = BK\dot{m}|\dot{m}| = 0 \tag{4}$$

(2) The heating model is mainly concerned with the supply of loads and the power balance before and after the mixing of nodes, which can be denoted as:

$$\boldsymbol{\varphi} = C_p \cdot \mathbf{m_q} \cdot (\mathbf{T_s} - \mathbf{T_o}) \tag{5}$$

$$T_{end} = (T_{start} - T_a) \cdot e^{-\lambda L / C_p \dot{m}} + T_a \tag{6}$$

$$\left(\sum \dot{\mathbf{m}}_{out}\right) \mathbf{T}_{out} = \sum \dot{\mathbf{m}}_{in} \mathbf{T}_{in} \tag{7}$$

The main connection of the heating system and power system is the CHP in LIES, and for the tidal flow calculation, it is sufficient to focus

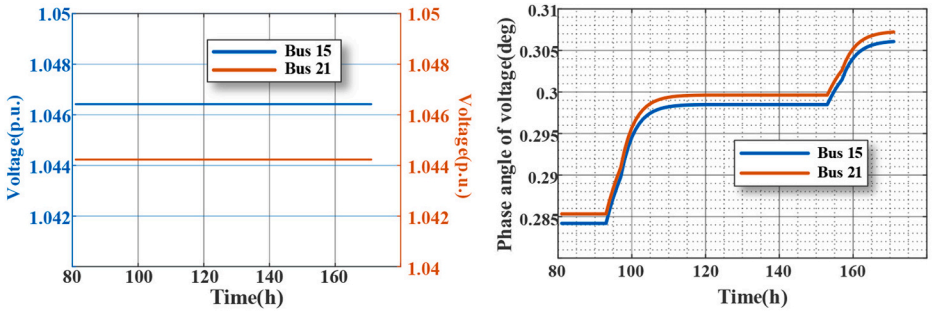

(a) Voltage amplitude of the buses (b) Phase angle of the buses

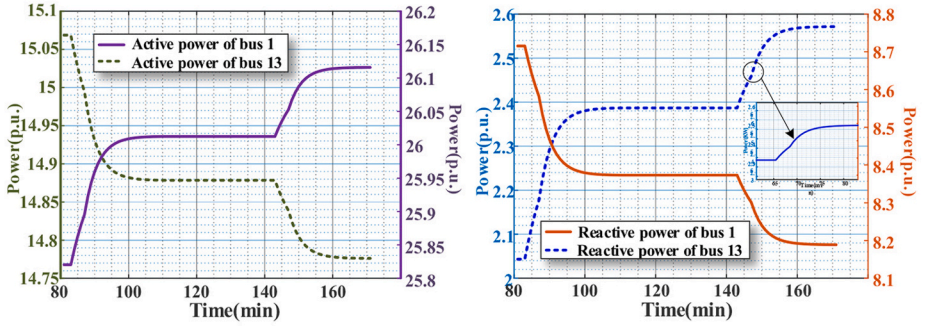

(c) Output of the active power (d) Output of the reactive power

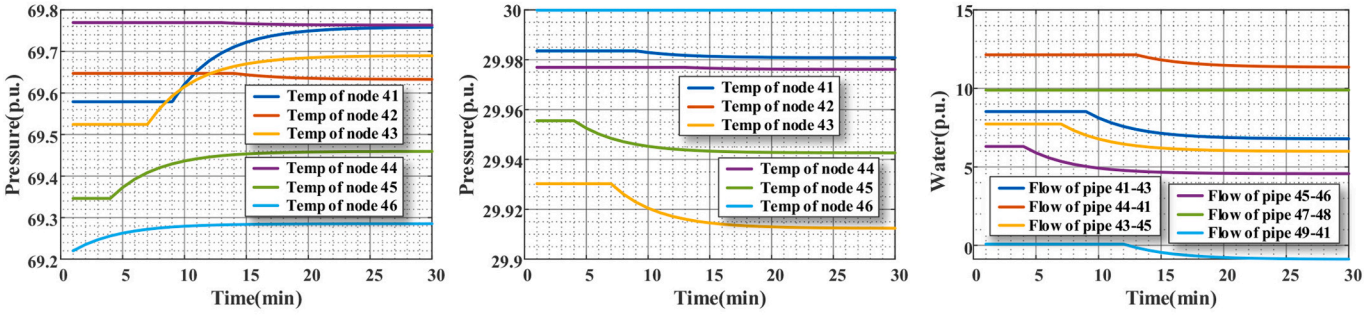

(e) Inlet temperature of the node (f) Outlet temperature of the node (g) Water flow of the pipe

Fig. 11. Calculation of the DEF in LIES.

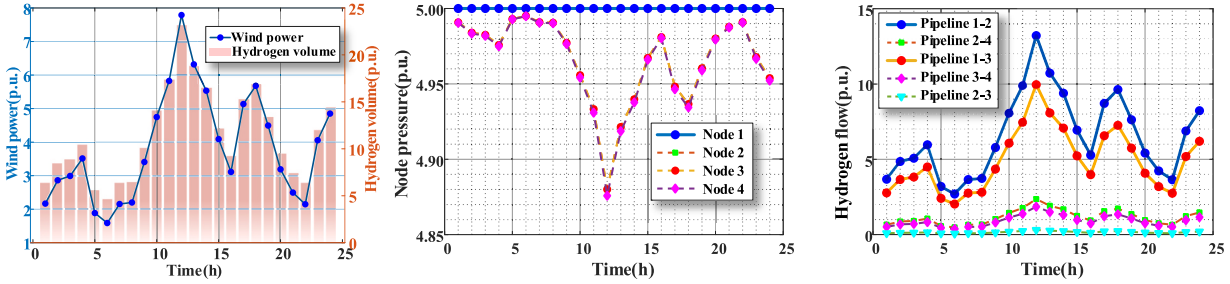

(a) Voltage amplitude of the buses (b) Hydrogen pressure of the nodes (c) Pipeline flow of the hydrogen

Fig. 12. Calculation of the DEF in CIES.

only on the power conversion, which can be represented as:

$$\phi_{\mathrm{CHP}} = P_{\mathrm{CHP},e} + \varphi_{\mathrm{CHP},h} \tag{8}$$

$$\gamma_{\mathrm{eh}} = \frac{\varphi_{\mathrm{CHP},h}}{P_{\mathrm{CHP},e}} \tag{9}$$

$$\phi_{\mathrm{CHP},min} \le \phi_{\mathrm{CHP}} \le \phi_{\mathrm{CHP},max} \tag{10}$$

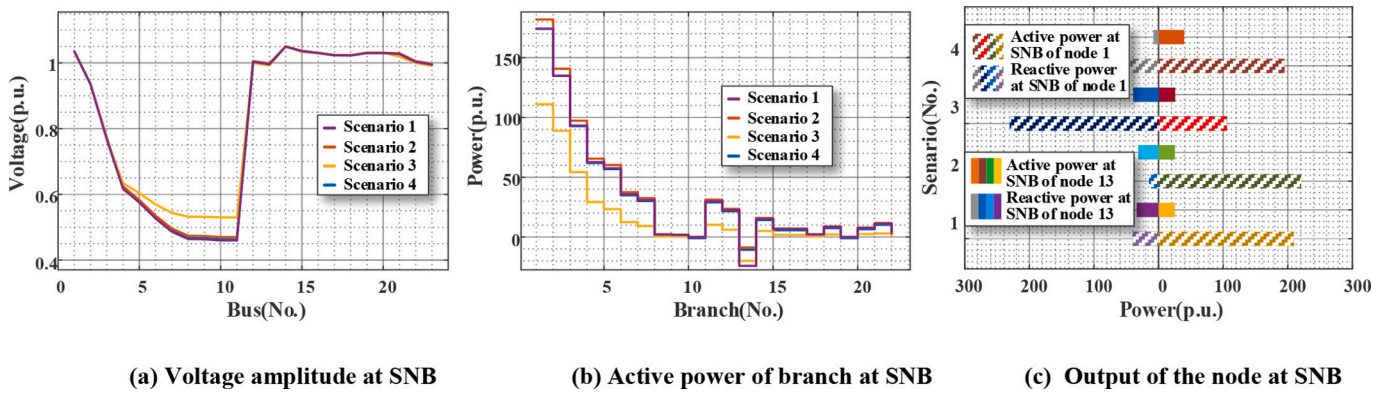

(a) Voltage amplitude at SNB (b) Active power of branch at SNB (c) Output of the node at SNB

Fig. 13. Calculation of the CEF in LIES.

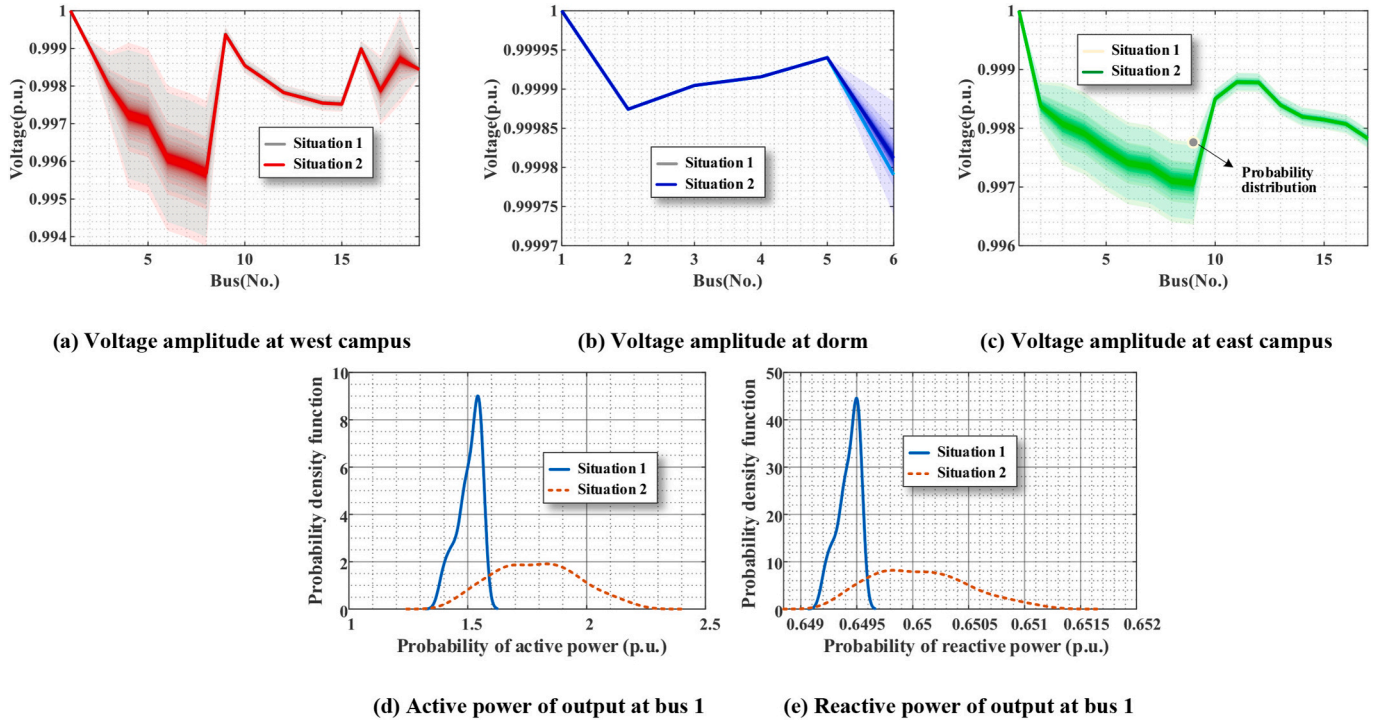

(a) Voltage amplitude at west campus (b) Voltage amplitude at dorm (c) Voltage amplitude at east campus

(d) Active power of output at bus 1 (e) Reactive power of output at bus 1

Fig. 14. Calculation of the PEF in CIES.

The power conversion is EB in CIES, and the energy balance equation can be represented as:

$$\varphi_{\mathrm{EB}} = \alpha \cdot H_g \cdot P_{\mathrm{EB}} \tag{11}$$

$$0 \le \varphi_{\mathrm{EB}} \le \varphi_{\mathrm{EB},max} \tag{12}$$

The system of nonlinear equations can be calculated using Newton's method [18].

4.2. Derivative research based on the energy flow

The proposed benchmarks are implemented in multiple scenarios for derivative research. These derivative studies involve optimal energy flow (OEF), probabilistic energy flow (PEF), continuous energy flow (CEF), and dynamic energy flow (DEF). Through combinations and integration, these investigations also support advanced applications.

(1) Optimal energy flow calculations [31]:

This paper remodels the energy flow model into an optimization model by adding operational boundaries and reformulating the objective function. The operation supports optimization for minimizing network losses, voltage control, and maximizing utilization of PV. The optimization may be applied globally or locally within benchmarked partitions. It is not limited to power flows but also regulates heating flows to optimize water temperature and flow rates for cost-efficiency. Such gains are especially prominent as the pipeline ages and degrades.

(2) Dynamic energy flow calculation [32]:

The alteration in energy flow performs as a dynamic process, complying with operational principles and laws inherent to a nonlinear dynamical system. The simulation enables the state variables \ perfectly captures system fluctuations, encompassing variations both from the load and PV. Thus, the test benchmarks need to be designed to support this functionality and align accurately with the system characteristics across various levels.

Table A-I
Bus data of LIES.

Bus	Type	Active load (p.u.)	Reactive load (p.u.)	Voltage (p.u.)	Phase angel (p.u.)	Voltage level (p.u.)
E1	3	0	0	1.008	0.171	66
E2	1	2.7	1.02	0.98	−2.414	10
E3	1	5	1.2	0.933	−3.04	10
E4	1	3.4	0.5	0.906	−4.103	10
E5	1	0.271	0.064	0.885	−4.563	10
E6	1	4.4	1.2	0.871	−5.312	10
E7	1	0.555	0.112	0.856	−6.193	10
E8	1	7.1	1.5	0.856	−6.224	10
E9	1	0.073	0.0259	0.856	−6.251	10
E10	1	0.4678	0.0432	0.856	−6.257	10
E11	1	0	0	0.974	−10.17	10
E12	1	0.84	0.24	1.015	−10.46	10
E13	1	2.87	0.18	0.979	−9.79	10
E14	2	0	0	0.988	−7.18	10
E15	1	1.93	0.13	1.013	−8.85	10
E16	1	0	0	1.017	−5.39	10
E17	1	1.152	0.45	1.001	−11.71	10
E18	1	0.5665	0.0276	0.97	−13.2	10
E19	1	2.1727	0.349	1.008	−12.89	10
E20	1	0	0	1.008	−12.91	10
E21	1	1.9335	1.1323	0.999	−13.25	10
E22	1	0.8435	0.4398	0.999	−13.25	10
E23	1	2.8797	1.3833	0.999	−13.25	10

Table A-II
Branch data of LIES.

Branch	BusF	BusT	R(p.u.)	X(p.u.)	B(p.u.)
B1	E1	E2	0.5055	0.28	0.0218
B2	E2	E3	0.9727	0.56	0
B3	E3	E4	1.0982	0.5182	0
B4	E4	E5	0.3782	0.1236	0
B5	E5	E6	0.4455	0.1636	0
B6	E6	E7	0.5473	0.2164	0
B7	E7	E8	0.3236	0.1	0
B8	E8	E9	0.1836	0.0855	0
B9	E9	E10	0.8327	0.4709	0
B10	E10	E11	1.3291	0.7564	0
B11	E1	E12	0.9291	0.5291	0.0255
B12	E12	E13	0.2836	0.1691	0
B13	E1	E14	0.6036	0.3364	0.0345
B14	E14	E15	0.8182	0.4582	0
B15	E1	E16	0.6364	0.3564	0.0273
B16	E16	E17	0.8836	0.4982	0
B17	E17	E18	0.3236	0.1927	0
B18	E1	E19	0.5218	0.2945	0.0236
B19	E15	E21	0.0673	0.04	0
B20	E13	E23	0.8855	0.5073	0
B21	E12	E22	0.0636	0.0309	0
B22	E19	E20	0.0622	0.0436	0

Table A-III
Power supply data of LIES.

Bus	Active ouput (p.u.)	Reactive ouput (p.u.)	Voltage (p.u.)	Phase angel (p.u.)	Max ouput (p.u.)
E1	15.58	1.11	1.035	0	50
E14	25.30	9.64	1.05	–	60

(3) Continuous energy flow calculation [33]:

The core concept of the CEF involves persistently calculating the energy flow with the load progressively increasing. The computation, starting from the current operational point and proceeding until the close of the bifurcation of voltage, employs a continuous prediction/calibration operator to account for the escalating load. This is an effective method to detect system's steady state and the designed LIES is available for this operation.

Table A-IV
Node data of LIES.

Node	Type	Load (p.u.)	Tin min (p.u.)	Tin max (p.u.)	Tout min (p.u.)	Tout max (p.u.)
H1	3	0	65	70	25	30
H2	1	0.5854	65	70	25	30
H3	1	0.9631	65	70	25	30
H4	1	0.3635	65	70	25	30
H5	1	0.1017	65	70	25	30
H6	1	0.3956	65	70	25	30
H7	1	0.5363	65	70	25	30
H8	1	0.9128	65	70	25	30
H9	1	0.2054	65	70	25	30
H10	1	0.0428	65	70	25	30
H11	1	0.2038	65	70	25	30
H12	1	0.2057	65	70	25	30
H13	1	0.8437	65	70	25	30
H14	1	0.3187	65	70	25	30
H15	1	0.3186	65	70	25	30
H16	1	0.2327	65	70	25	30
H17	1	0.7703	65	70	25	30
H18	1	1.0781	65	70	25	30
H19	1	0.8859	65	70	25	30
H20	1	0.9734	65	70	25	30
H21	1	0.2761	65	70	25	30
H22	1	0.2493	65	70	25	30
H23	1	0.4573	65	70	25	30
H24	1	0.3001	65	70	25	30
H25	1	0.3709	65	70	25	30
H26	1	1.9529	65	70	25	30
H27	1	0.5854	65	70	25	30
H28	1	0.4724	65	70	25	30
H29	1	0.1616	65	70	25	30
H30	1	3.1184	65	70	25	30
H31	1	0.4334	65	70	25	30
H32	1	0.9534	65	70	25	30
H33	1	1.4945	65	70	25	30
H34	1	0.3882	65	70	25	30
H35	1	0.1714	65	70	25	30
H36	1	1.0312	65	70	25	30
H37	1	0.5654	65	70	25	30
H38	1	0.3354	65	70	25	30
H39	1	0.2566	65	70	25	30
H40	1	0.8189	65	70	25	30
H41	1	0.6125	65	70	25	30
H42	1	1.1465	65	70	25	30
H43	1	0.1314	65	70	25	30
H44	1	1.8372	65	70	25	30
H45	1	0.2352	65	70	25	30
H46	1	1.0335	65	70	25	30
H47	1	0.0512	65	70	25	30
H48	1	1.6435	65	70	25	30
H49	1	0.0561	65	70	25	30
H50	1	0.1345	65	70	25	30
H51	1	0.0936	65	70	25	30
H52	1	1.8294	65	70	25	30
H53	1	0.5032	65	70	25	30

(4) Probabilistic energy flow calculation [34]:

As the proportion of renewable energy sources and load fluctuations, PEF has emerged as a pivotal tool in mainstream research. PEF is instrumental in evaluating the probability distribution of a system's state. The design needs to imperative for match the application of PEF with the installation of the PV and other possible distributed generation.

Most of advanced technologies are motivated by basic energy flow and derivative research. Additionally, there exists a multitude of other analogous computations that are beyond the scope of this listing. The test benchmarks outlined in this study provide a versatile fundamental research for various advanced applications. These calculations may be extended to energy management [35], reliability evaluation [36],

Table A-V
Pipeline data of LIES.

Pipe	NodeF	NodeT	Length (p.u.)	Diameter (p.u.)	Coefficient (p.u.)	efficiency (p.u.)
P1	H1	H2	250	80	0.321	0.4
P2	H1	H4	200	300	0.21	0.4
P3	H1	H29	150	180	0.21	0.4
P4	H2	H3	350	80	0.327	0.4
P5	H4	H5	100	180	0.13	0.4
P6	H4	H6	250	80	0.23	0.4
P7	H4	H9	150	240	0.21	0.4
P8	H5	H19	400	80	0.21	0.4
P9	H5	H53	350	180	0.21	0.4
P10	H6	H8	250	80	0.327	0.4
P11	H7	H28	200	80	0.21	0.4
P12	H9	H10	150	240	0.327	0.4
P13	H10	H11	200	240	0.327	0.4
P14	H11	H13	300	100	0.219	0.4
P15	H11	H35	120	180	0.189	0.4
P16	H12	H7	250	80	0.189	0.4
P17	H13	H12	200	100	0.189	0.4
P18	H14	H15	200	80	0.278	0.4
P19	H16	H20	300	80	0.189	0.4
P20	H16	H22	150	80	0.189	0.4
P21	H20	H21	200	80	0.236	0.4
P22	H22	H23	200	80	0.189	0.4
P23	H26	H25	350	80	0.189	0.4
P24	H27	H16	200	100	0.236	0.4
P25	H27	H17	250	80	0.189	0.4
P26	H27	H18	250	80	0.189	0.4
P27	H27	H24	300	80	0.21	0.4
P28	H27	H26	400	100	0.189	0.4
P29	H28	H14	200	80	0.189	0.4
P30	H29	H30	100	80	0.321	0.4
P31	H30	H50	150	100	0.321	0.4
P32	H31	H34	350	100	0.321	0.4
P33	H34	H32	350	80	0.189	0.4
P34	H34	H33	350	80	0.21	0.4
P35	H35	H36	250	80	0.189	0.4
P36	H35	H37	300	180	0.321	0.4
P37	H37	H38	150	180	0.189	0.4
P38	H38	H39	150	80	0.327	0.4
P39	H38	H40	350	180	0.321	0.4
P40	H40	H52	350	180	0.21	0.4
P41	H41	H43	120	80	0.23	0.4
P42	H44	H41	350	100	0.21	0.4
P43	H43	H45	250	80	0.327	0.4
P44	H45	H46	250	80	0.189	0.4
P45	H47	H48	300	80	0.189	0.4
P46	H49	H41	300	100	0.236	0.4
P47	H49	H42	150	80	0.321	0.4
P48	H50	H51	150	100	0.23	0.4
P49	H51	H31	300	100	0.327	0.4
P50	H40	H47	100	100	0.189	0.4
P51	H47	H49	150	180	0.189	0.4
P52	H53	H27	300	180	0.189	0.4
P53	H15	H44	300	180	0.189	0.4

calculation of available transmission capacity [37], and security calibrations. Each of these studies leverages advancements in optimization and dynamic analysis. The inherent adaptability of benchmarks empowers them to be particularly suitable for testing and available evaluating advanced technologies. This flexibility not only facilitates comprehensive experimentation but also plays a pivotal role in advancing the standardization of these technologies.

5. Case studies

In this section, the visualization of calculations for foundational energy flow and derivative research of the benchmark are shown and demonstrated the availability and functionality of the test benchmarks.

Table B-I
Bus data of CIES.

Bus	Type	Active load (p.u.)	Reactive load (p.u.)	Voltage level (p.u.)	Area
e1	3	0	0	10,000	1
e2	1	0	0	220	1
e3	1	99.85	56.65	220	1
e4	1	87.36	37.43	220	1
e5	1	89.84	38.4	220	1
e6	1	195.86	95.48	220	1
e7	1	198.3	94.61	220	1
e8	1	415.77	195.63	220	1
e9	1	58.77	17.56	220	1
e10	1	57.09	14.37	220	1
e11	1	55.31	18.47	220	1
e12	1	119.76	76.8	220	1
e13	1	119.73	74.27	220	1
e14	1	419.9	198.39	220	1
e15	1	86.59	38.5	220	1
e16	1	57.01	29.43	220	1
e17	1	199.43	99.59	220	1
e18	1	416.02	198.2	220	1
e19	1	196.91	96.45	220	1
e20	3	0	0	10,000	2
e21	1	119.65	76.18	220	2
e22	1	209.32	95.21	220	2
e23	1	196.06	96.99	220	2
e24	1	119.54	76.1	220	2
e25	1	198.81	95.22	220	2
e26	3	0	0	10,000	3
e27	1	89.48	36.39	220	3
e28	1	115.71	79.33	220	3
e29	1	116.51	76.91	220	3
e30	1	116.33	74.97	220	3
e31	1	116.75	74.48	220	3
e32	1	117.42	77.01	220	3
e33	1	118.37	78.33	220	3
e34	1	116.69	76.08	220	3
e35	1	239.41	154.5	220	3
e36	1	59.26	16.94	220	3
e37	1	59.9	14.15	220	3
e38	1	115.18	78.82	220	3
e39	1	55.15	19.33	220	3
e40	1	59.38	18.22	220	3
e41	1	197.66	97.62	220	3
e42	1	236.72	157.48	220	3

5.1. Energy flow calculation

This section calculated the EF of LIES and CIES via Newton's method [38].

1) *LIES benchmark*

The EF for LIES has been implemented and the results are exhibited in Fig. 6. The base quantities of the energy transferred are set at 1 MW and 1 MVAR in the electric system and 100 m/s for the pipe in the heating system.

The buses' voltage and phase angle and the branches' power are illustrated in Fig. 6 (a) - Fig. 6 (c). From Fig. 6(a) and (b), with energy transmission, there is a noticeable downward trend in both voltage and phase angle. In Fig. 6(c), the location of the CHP is a negative value to showcase the output power. Additionally, the temperature of nodes and the water flow in pipes are compiled and presented in Fig. 6 (d) and Fig. 6 (e). From Fig. 6(d), the reduction of inlet water temperature is marked by a decrease within 2% at all nodes, while the return water temperature shows a decline within 1%. Lastly, Fig. 6(e) gathers the pipe water flow values, revealing a distribution that aligns with Kirchhoff's law [39]. All loads have matching supplies in LIES.

2) *CIES benchmark*

Table B-II
Branch data of CIES.

Branch	BusF	BusT	R(p.u.)	X(p.u.)	Branch	BusF	BusT	R(p.u.)	X(p.u.)
b1	e1	e2	0.0477	0.0228	b22	e20	e24	0.0391	0.0172
b2	e2	e16	0.0166	0.0088	b23	e20	e25	0.0817	0.0492
b3	e2	e3	0.0505	0.0229	b24	e26	e36	0.0413	0.0207
b4	e3	e17	0.0392	0.0227	b25	e36	e35	0.0915	0.0431
b5	e3	e4	0.044	0.0273	b26	e36	e37	0.0126	0.0061
b6	e4	e5	0.0129	0.0096	b27	e36	e27	0.0244	0.014
b7	e5	e6	0.0982	0.0478	b28	e27	e28	0.0202	0.0091
b8	e6	e7	0.0216	0.0132	b29	e28	e29	0.0173	0.0092
b9	e7	e8	0.0443	0.022	b30	e29	e30	0.0354	0.0165
b10	e1	e9	0.0234	0.0095	b31	e30	e31	0.0366	0.0192
b11	e9	e18	0.0658	0.0442	b32	e31	e32	0.0137	0.0071
b12	e9	e10	0.0593	0.0381	b33	e32	e33	0.0773	0.035
b13	e10	e19	0.0413	0.0181	b34	e33	e34	0.0292	0.0137
b14	e10	e11	0.036	0.0155	b35	e36	e38	0.0434	0.0279
b15	e11	e12	0.0397	0.0172	b36	e38	e39	0.0285	0.0143
b16	e12	e13	0.017	0.0091	b37	e39	e40	0.008	0.0041
b17	e13	e14	0.0226	0.0112	b38	e40	e41	0.0122	0.0074
b18	e14	e15	0.0273	0.0146	b39	e41	e42	0.0729	0.0462
b19	e20	e21	0.0748	0.0475	b40	e23	e3	0.0817	0.0492
b20	e20	e22	0.0372	0.0184	b41	e42	e15	0.0729	0.0462
b21	e20	e23	0.0336	0.0191					

Table B-III
Photovoltaic and energy storage data of CIES.

Bus	PV	ESS	Installed capacity(p.u.)	Maximum capacity(p.u.)	Max output(p.u.)	Efficiency (p.u.)
e4	√		0.4	–	–	–
e9	√		0.35	–	–	–
e18	√		0.35	–	–	–
e28	√		0.2	–	–	–
e17		√	–	1.5	0.125	0.9
e33		√	–	2	0.125	0.9

The results of EF for the power and heating systems of the CIES have been shown in Fig. 7.

Fig. 7(a) depicts the voltage distribution across the three campuses. Fig. 7(b) illustrates both active and reactive power of the branches across the three campuses. Fig. 7(c) focuses on the heating power output of the pipe network, each campus is heated by two primary pipes. Fig. 7 (d) presents the temperatures at the inlet and outlet points of the water system. Fig. 7(e) visualizes the heat flow distribution, offering insights into the heating water and energy movement within the system. These results support to understand the state of the system.

The coordination of electricity and heat exchange across the entire region is balanced, and all demands were met without any deficits in electricity or heat provision. This outcome demonstrates the basic benchmark in efficiently distributing the energy supply and demand among different regions, ensuring the stable operation of the energy system.

In this section, the computations have successfully quantified all foundational energy flow. The results presented only reflect the base state of IES with the condition that system loads and other parameters are constants. In the real-world system, loads are constantly evolving demands that test benchmarks have more robust capabilities to enable various types of calculations to be implemented. This dynamic property requires more advanced computational tools and access and modification for benchmarks. The benchmark has now progressed to encompass a range of derivative studies, expanding the scope and depth of analysis.

5.2. Derivative research of energy flow calculation

Derivative energy flow research may re-schedule and enhance the performance of energy flow with myriad conditions. It is further demonstrated that all databases can be accessed and modified with various conditions. The new strategy may be applied to LIES and CIES.

3) *Scalable EF with P2H Planning*

In this study, the EF also take into account utility planning for wind power and hydrogen stations. Bus 12 is a candidate to connect 6 wind turbines, each with an installed capacity of 2 MW. The P2H maintains a base pressure of 70 bar. The base quantities of the hydrogen pressure is set at 10 bar and the hydrogen volume is set at 1 m^3. For this scenario, the energy flow requires a hydrogen system. The results are shown in Fig. 8.

The Fig.8. showcases EF in CIES with wind power and hydrogen system. Wind power is converted to hydrogen via a P2H in Fig.8(a). Pipelines transport hydrogen efficiently, with a larger value in the main pipelines in Fig.8(b). Surplus wind power feeds into the power system, and branch power analysis reveals increased active and reactive power of branch 11, demonstrating improved renewable energy utilization.

4) *OEF*

With the evolving utilization, the insulation layers within pipes undergo natural aging and degradation. This demands a recalibration of operational strategies to maintain system efficiency. The programming resets the computational objective of OEF to optimal economic dispatch. The OEF results are shown in Fig. 9- Fig. 10.

After OEF, this section re-scheduled the output of the heat system, increasing the total output and the incoming water flow to the nodes. This strategy applies to every test benchmark. As demonstrated in Fig. 9 (a), the implementation of the OEF creates an enhancement of the node voltage. Concurrently, Fig. 9(b) illustrates a reduction in the inflow-outflow water temperature at the node, whereas Fig. 9(c) depicts an increase in the water flow rate. These figures collectively highlight the multifaceted impacts of the optimization strategy on the system's operational parameters.

Fig. 10 elucidates the water flow dynamics at each node across the three campuses. Bus voltage variations within the CIES are notably minor without further elaboration. Furthermore, the observed temperature trends are closely aligned with the LIES, indicating a similar trend in heating systems.

The primary mission of OEF is to address the degradation of pipe insulation within heating systems in this paper. Notably, these re-schedules maintain the energy supply with minimal energy

Table B-IV
Node data of CIES.

Node	Type	Load(p.u.)	Tin min(p.u.)	Tin max(p.u.)	Tout min(p.u.)	Tout max(p.u.)	Area
h1	3	0	60	70	25	30	1
h2	1	0.2255	60	70	25	30	1
h3	1	0.0545	60	70	25	30	1
h4	1	0.0344	60	70	25	30	1
h5	1	0.3333	60	70	25	30	1
h6	1	0.0305	60	70	25	30	1
h7	1	0.0165	60	70	25	30	1
h8	1	0.0165	60	70	25	30	1
h9	1	0.0429	60	70	25	30	1
h10	1	0.0429	60	70	25	30	1
h11	1	0.0275	60	70	25	30	1
h12	1	0.0759	60	70	25	30	1
h13	1	0.0512	60	70	25	30	1
h14	1	0.1073	60	70	25	30	1
h15	1	0.0361	60	70	25	30	1
h16	1	0.0083	60	70	25	30	1
h17	1	0.0176	60	70	25	30	1
h18	1	0.0132	60	70	25	30	1
h19	1	0.0083	60	70	25	30	1
h20	1	0.1364	60	70	25	30	1
h21	1	0.099	60	70	25	30	1
h22	1	0.1225	60	70	25	30	1
h23	2	0	66	70	25	30	1
h24	3	0	60	70	25	30	2
h25	1	0.0404	60	70	25	30	2
h26	1	0.0404	60	70	25	30	2
h27	1	0.0371	60	70	25	30	2
h28	1	0.0396	60	70	25	30	2
h29	1	0.0832	60	70	25	30	2
h30	1	0.026	60	70	25	30	2
h31	1	0.026	60	70	25	30	2
h32	1	0.0227	60	70	25	30	2
h33	1	0.0346	60	70	25	30	2
h34	1	0.0291	60	70	25	30	2
h35	1	0.0404	60	70	25	30	2
h36	1	0.0433	60	70	25	30	2
h37	1	0.0118	60	70	25	30	2
h38	1	0.0404	60	70	25	30	2
h39	1	0.0404	60	70	25	30	2
h40	2	0	60	70	25	30	2
h41	3	0	60	70	25	30	3
h42	1	0.0143	60	70	25	30	3
h43	1	0.0275	60	70	25	30	3
h44	1	0.1628	60	70	25	30	3
h45	1	0.0309	60	70	25	30	3
h46	1	0.0385	60	70	25	30	3
h47	1	0.1386	60	70	25	30	3
h48	1	0.1386	60	70	25	30	3
h49	1	0.297	60	70	25	30	3
h50	1	0.099	60	70	25	30	3
h51	1	0.1155	60	70	25	30	3
h52	2	0	60	70	25	30	3

consumption. Another benefit observed is an increase in voltage, a conclusion predominantly highlighted in LIES.

5) *DEF*

The test benchmarks also contribute to a dynamic evolution of the power flow influenced by cyclical load variations. Additionally, this section has quantified the dynamic trends of temperature at various nodes and consolidated these data in Fig. 11. The load at node 46 is configured to correlate with the temperature changes. This load may be transmitted to the power system. This section utilizes simulation to analyze and delineate the trends in the temperature of the nodes and the water flow of the pipes.

As shown in Fig. 11(a)-(b), the electrical loads follow the temperature change and the voltage change is minimal since their power does not change much compared to the entire network. The phase angle, on the other hand, shows similar results to the variation in the thermal load. The main transformer regulates the output to compensate for the power demand, owing to the operating predominantly in heating-based electricity mode in Fig. 11 (c) - (d). Specifically, in Fig. 11 (d), there are two distinct sets of water pipes from node 46 to node 1, leading to a knot in the process of multi-temporal load variation, attributing to the differing lengths of this water pipe path. The system exhibited temporal temperature and water flow rate variations in Fig. 11 (e) - (g). The load is observed to propagate to the CHP, increasing its power output after 30 min than the load variation.

Additionally, DEF may compute with variations in wind power output at the hourly level. The wind power captures wind speed, while the output of hydrogen and other state parameters change concurrently, as illustrated in Fig. 12.

Fig. 12 illustrates various aspects of the wind power and hydrogen production system. Fig. 12 (a) shows the correlation between wind power output and hydrogen volume over 24 h, indicating that hydrogen volume fluctuates in response to wind power variations. Fig. 12 (b) displays hydrogen node pressure variations, highlighting the fluctuations in the hydrogen system. Fig. 12 (c) represents hydrogen flow through various pipelines, demonstrating the impact of wind power on hydrogen distribution in the system.

6) *CEF*

Continuous energy flow is commonly employed to calculate secure operational borders within a system. The results of this computation for LIES are showcased in Fig. 13. Set four scenarios to compare:

Scenario 1: Increase active and reactive loads to calculate SNB.

Scenario 2: Increase only active loads to calculate SNB.

Scenario 3: Increase only reactive loads to calculate SNB.

Scenario 4: Increase active and reactive power to calculate SNB with heating load increase.

As observed in Fig. 13(a) and (b), the minimum voltage for the four scenarios may decrease to below 0.5 p.u. at SNB. Notably, increasing the reactive power tends to enable the operation state of the system more rapidly towards the SNB point, and a similar trend is evidently in the branch. Fig. 12(c) delineates the distribution of active and reactive power output. The influence of the heat network on the SNB is primarily manifested through variations in the output power at the heat source node.

7) *PEF*

Probabilistic energy flows serve as a critical analytical tool for assessing the probability distributions of state variables in CIES. To this end, this section has methodically structured two experimental sets for comparative analysis:

Situation 1: This experiment involves probabilistic currents calculated without incorporating the heat network.

Situation 2: This set accounts for the heat network while analyzing probabilistic flow dynamics.

Fig. 14 showcases the visualization of the probability distribution for all nodes through the PEF computations. Notably, the fluctuation range of these probability distributions diminishes with the heat load increases. This results in a more tightly concentrated distribution around the mean value, indicating a more predictable and stable system behavior under these conditions.

As can be seen, test benchmarks can perform all basic and derived calculations, in addition to other advanced applications not listed in this paper [39–42]. More functions remain to be explored by the readers.

6. Conclusion

This paper introduces a real-world benchmark synopsis and energy flow calculations, aiming to contribute a typical test case from real-

Table B-V
Pipeline data of CIES.

Pipe	Area	Intra-area pipe No.	NodeF	NodeT	Length(p.u.)	Diameter(p.u.)	Coefficient(p.u.)	Efficiency(p.u.)
p1	1	pw1	h1	h2	30	40	0.321	0.4
p2	1	pw2	h2	h3	120	40	0.21	0.4
p3	1	pw3	h3	h4	30	40	0.21	0.4
p4	1	pw4	h3	h5	50	40	0.327	0.4
p5	1	pw5	h5	h6	100	40	0.13	0.4
p6	1	pw6	h6	h7	50	40	0.23	0.4
p7	1	pw7	h6	h8	50	40	0.21	0.4
p8	1	pw8	h9	h5	120	40	0.21	0.4
p9	1	pw9	h9	h10	20	40	0.21	0.4
p10	1	pw10	h10	h11	60	40	0.327	0.4
p11	1	pw11	h12	h9	40	40	0.21	0.4
p12	1	pw12	h13	h12	120	40	0.327	0.4
p13	1	pw13	h13	h14	60	40	0.327	0.4
p14	1	pw14	h13	h15	100	40	0.219	0.4
p15	1	pw15	h15	h16	50	40	0.189	0.4
p16	1	pw16	h15	h17	60	40	0.189	0.4
p17	1	pw17	h15	h18	50	40	0.189	0.4
p18	1	pw18	h18	h19	20	40	0.278	0.4
p19	1	pw19	h19	h20	130	40	0.189	0.4
p20	1	pw20	h20	h21	120	40	0.189	0.4
p21	1	pw21	h22	h21	140	40	0.236	0.4
p22	1	pw22	h2	h22	30	40	0.189	0.4
p23	1	pw23	h23	h13	30	40	0.189	0.4
p24	2	pe1	h24	h25	30	40	0.321	0.4
p25	2	pe2	h25	h26	40	40	0.21	0.4
p26	2	pe3	h26	h27	30	40	0.21	0.4
p27	2	pe4	h27	h28	30	40	0.327	0.4
p28	2	pe5	h27	h30	100	40	0.13	0.4
p29	2	pe6	h30	h29	50	40	0.23	0.4
p30	2	pe7	h30	h31	80	40	0.21	0.4
p31	2	pe8	h33	h31	40	40	0.21	0.4
p32	2	pe9	h33	h32	100	40	0.21	0.4
p33	2	pe10	h36	h33	40	40	0.327	0.4
p34	2	pe11	h36	h35	100	40	0.21	0.4
p35	2	pe12	h36	h34	100	40	0.327	0.4
p36	2	pe13	h39	h36	40	40	0.327	0.4
p37	2	pe14	h39	h38	100	40	0.219	0.4
p38	2	pe15	h39	h37	130	40	0.189	0.4
p39	2	pe16	h40	h39	150	40	0.219	0.4
p40	2	pe17	h40	h24	150	40	0.219	0.4
p41	3	pd1	h41	h42	40	40	0.321	0.4
p42	3	pd2	h42	h43	220	40	0.21	0.4
p43	3	pd3	h43	h44	40	40	0.21	0.4
p44	3	pd4	h44	h45	30	40	0.327	0.4
p45	3	pd5	h45	h46	50	40	0.13	0.4
p46	3	pd6	h44	h47	140	40	0.23	0.4
p47	3	pd7	h47	h48	120	40	0.21	0.4
p48	3	pd8	h48	h49	110	40	0.21	0.4
p49	3	pd9	h50	h49	90	40	0.21	0.4
p50	3	pd10	h51	h50	50	40	0.327	0.4
p51	3	pd11	h52	h51	450	40	0.327	0.4
p52	3	pd12	h52	h41	450	40	0.327	0.4

world IES in China. The test benchmark incorporates two scenarios: LIES and CIES, each with distinct heat network and power grid structures. This paper presents trend simulations from this test system, providing a comparative benchmark to evaluate the accuracy and feasibility of various integrated energy system studies. The benchmarking system encompasses a comprehensive set of parameters, including feeder specifications, load characteristics, and distributed power output profiles for multiple distributed power sources. The proposed benchmark testing system structure can be tailored to address scenarios typical of integrated energy systems with explosive development and high penetration rates. As the economy and technology continue to evolve, integrated energy systems with advanced energy conversion technologies will become increasingly prevalent. This benchmark test system allows experts and researchers to adapt and update system parameters according to their specific research requirements and the evolving landscape of integrated energy systems.

CRediT authorship contribution statement

Xue Li: Investigation, Conceptualization. **Junyan Shao:** Writing – original draft, Software. **Tao Jiang:** Data curation, Conceptualization. **Houhe Chen:** Writing – review & editing, Supervision. **Yue Zhou:** Validation. **Rufeng Zhang:** Writing – review & editing, Visualization. **Hongjie Jia:** Writing – review & editing, Investigation. **Jianzhong Wu:** Writing – review & editing, Project administration.

Declaration of competing interest

The authors declare that they have no known competing financial interests or personal relationships that could have appeared to influence the work reported in this paper.

Data availability

The data that has been used is confidential.

Acknowledgments

This work is supported in part by the National Natural Science Foundation of China General Project (Grant No. 52077029, 52077028 and 52377080), National Natural Science Foundation of China International Cooperation and Exchange Project (Grant No. 52061635103), Natural Science Foundation of Jilin Province (Grant No. YDZJ202101-ZYTS194), Jilin Province Science and Technology Development Plan Project (No. 20200403066SF).

Appendix A. Appendix

See Tables A-I–A-V.

Appendix B. Appendix

See Tables B-I–B-V.

References

[1] Ma J, Yang L, Wang D, et al. Digitalization in response to carbon neutrality: mechanisms, effects and prospects[J]. Renew Sust Energ Rev 2024;191:114138.
[2] Wang W, Yuan B, Sun Q, et al. Application of energy storage in integrated energy systems—a solution to fluctuation and uncertainty of renewable energy[J]. J Energy Storage 2022;52:104812.
[3] Zhu J, Dong H, Zheng W, et al. Review and prospect of data-driven techniques for load forecasting in integrated energy systems[J]. Appl Energy 2022;321:119269.
[4] Hoang AT, Nguyen XP. Integrating renewable sources into energy system for smart city as a sagacious strategy towards clean and sustainable process[J]. J Clean Prod 2021;305:127161.
[5] Li P, Wang Z, Wang J, et al. A multi-time-space scale optimal operation strategy for a distributed integrated energy system[J]. Appl Energy 2021;289:116698.
[6] Guo Z, Zhang R, Wang L, et al. Optimal operation of regional integrated energy system considering demand response[J]. Appl Therm Eng 2021;191:116860.
[7] Lund H, Thorsen JE, Jensen SS, et al. Fourth-generation district heating and motivation tariffs[J]. ASME Open J Eng 2022;1(01):1002.
[8] Dang L, Chen B, Wang S, et al. Robust power system state estimation with minimum error entropy unscented Kalman filter[J]. IEEE Trans Instrum Meas 2020;69(11):8797–808.
[9] Li Y, Wang C, Li G, et al. Improving operational flexibility of integrated energy system with uncertain renewable generations considering thermal inertia of buildings[J]. Energy Convers Manag 2020;207:112526.
[10] Kamruzzaman M, Duan J, Shi D, et al. A deep reinforcement learning-based multi-agent framework to enhance power system resilience using shunt resources[J]. IEEE Trans Power Syst 2021;36(6):5525–36.
[11] Qin X, Shen X, Guo Y, et al. Combined electric and heat system testbeds for power flow analysis and economic dispatch[J]. CSEE J Power Energy Syst 2020;7(1):34–44.
[12] Egeland-Eriksen T, Hajizadeh A, Sartori S. Hydrogen-based systems for integration of renewable energy in power systems: achievements and perspectives[J]. Int J Hydrog Energy 2021;46(63):31963–83.
[13] Dong X, Liu L, Musial K, et al. Nats-bench: benchmarking nas algorithms for architecture topology and size[J]. IEEE Trans Pattern Anal Mach Intell 2021;44(7):3634–46.
[14] Zhu J, Dong H, Zheng W, et al. Review and prospect of data-driven techniques for load forecasting in integrated energy systems[J]. Appl Energy 2022;321:119269.
[15] Li P, Wang Z, Wang J, et al. A multi-time-space scale optimal operation strategy for a distributed integrated energy system[J]. Appl Energy 2021;289:116698.
[16] Ding J, Xue N, Xia GS, et al. Object detection in aerial images: a large-scale benchmark and challenges[J]. IEEE Trans Pattern Anal Mach Intell 2021;44(11):7778–96.
[17] Dolatabadi SH, Ghorbanian M, Siano P, et al. An enhanced IEEE 33 bus benchmark test system for distribution system studies[J]. IEEE Trans Power Syst 2020;36(3):2565–72.
[18] Liu R, Fan X, Zhu M, et al. Real-world underwater enhancement: challenges, benchmarks, and solutions under natural light[J]. IEEE Trans Circuits Syst Video Technol 2020;30(12):4861–75.
[19] Khemraj C, Sharma A, Kuldeep BS. Using a Meta heuristic algorithm, design simulation of improved optimal power flow in IEEE-118 bus system[J]. Int J Digital Electron 2021;7(2):19–28.
[20] Kamruzzaman M, Duan J, Shi D, et al. A deep reinforcement learning-based multi-agent framework to enhance power system resilience using shunt resources[J]. IEEE Trans Power Syst 2021;36(6):5525–36.
[21] Long Y, Xia GS, Li S, et al. On creating benchmark dataset for aerial image interpretation: reviews, guidances, and million-aid[J]. IEEE J Selected Topics Appl Earth Observ Remote Sens 2021;14:4205–30.
[22] Su C, Dalgren J, Palm B. High-resolution mapping of the clean heat sources for district heating in Stockholm City[J]. Energy Convers Manag 2021;235:113983.
[23] Narula K, de Oliveira Filho F, Villasmil W, et al. Simulation method for assessing hourly energy flows in district heating system with seasonal thermal energy storage [J]. Renew Energy 2020;151:1250–68.
[24] Calise F, Cappiello FL, d'Accadia MD, et al. Energy efficiency in small districts: dynamic simulation and techno-economic analysis[J]. Energy Convers Manag 2020;220:113022.
[25] Guo F, Zhu X, Zhang J, et al. Large-scale living laboratory of seasonal borehole thermal energy storage system for urban district heating[J]. Appl Energy 2020;264:114763.
[26] Xiong L, Liu X, Liu Y, et al. Modeling and stability issues of voltage-source converter-dominated power systems: a review[J]. CSEE J Power Energy Syst 2020;8(6):1530–49.
[27] Zhang T, Zheng W, Wang L, et al. Experimental study and numerical validation on the effect of inclination angle to the thermal performance of solar heat pipe photovoltaic/thermal system[J]. Energy 2021;223:120020.
[28] Nguyen HT, Safder U, Nguyen XQN, et al. Multi-objective decision-making and optimal sizing of a hybrid renewable energy system to meet the dynamic energy demands of a wastewater treatment plant[J]. Energy 2020;191:116570.
[29] Zhang Y, Pei X, Yang M, et al. Current-limiting strategy for asymmetric short-circuit of three-phase inverter for continuous power supply of non-faulty loads[J]. IEEE Trans Power Electron 2023;38(10):12620–33.
[30] Pordanjani AH, Aghakhani S, Afrand M, et al. Nanofluids: physical phenomena, applications in thermal systems and the environment effects-a critical review[J]. J Clean Prod 2021;320:128573.
[31] Farrokhifar M, Aghdam FH, Alahyari A, et al. Optimal energy management and sizing of renewable energy and battery systems in residential sectors via a stochastic MILP model[J]. Electr Power Syst Res 2020;187:106483.
[32] Akkurt GG, Aste N, Borderon J, et al. Dynamic thermal and hygrometric simulation of historical buildings: critical factors and possible solutions[J]. Renew Sust Energ Rev 2020;118:109509.
[33] Awaysheh FM, Aladwan MN, Alazab M, et al. Security by design for big data frameworks over cloud computing[J]. IEEE Trans Eng Manag 2021;69(6):3676–93.
[34] Li H, Hou K, Xu X, et al. Probabilistic energy flow calculation for regional integrated energy system considering cross-system failures[J]. Appl Energy 2022;308:118326.
[35] Jia W, Ding T, Huang C, et al. Convex optimization of integrated power-gas energy flow model with applications to probabilistic energy flow[J]. IEEE Trans Power Syst 2020;36(2):1432–41.
[36] Jiang T, Sun T, Liu G, et al. Resilience evaluation and enhancement for island city integrated energy systems[J]. IEEE Trans Smart Grid 2022;13(4):2744–60.
[37] Eidiani M, Zeynal H. An effective method to determine the available transmission capacity with variable frequency transformer[J]. Int Trans Electr Energy Syst 2023;2023(1):8404284.
[38] Zhang Y, Wang J, Chen B. Detecting false data injection attacks in smart grids: a semi-supervised deep learning approach[J]. IEEE Trans Smart Grid 2020;12(1):623–34.
[39] Shayegan KJ, Biswas S, Zhao B, et al. Direct observation of the violation of Kirchhoff's law of thermal radiation[J]. Nat Photonics 2023;17(10):891–6.
[40] Frizzo Stefenon S, Waldrigues Branco N, Nied A, et al. Analysis of training techniques of ANN for classification of insulators in electrical power systems[J]. IET Gener Transm Distrib 2020;14(8):1591–7.
[41] Li H, Lu Z, Qiao Y, et al. The flexibility test system for studies of variable renewable energy resources[J]. IEEE Trans Power Syst 2020;36(2):1526–36.
[42] Alimi OA, Ouahada K, Abu-Mahfouz AM. A review of machine learning approaches to power system security and stability[J]. IEEE Access 2020;8:113512–31.